CHEMISTRY OF MATERIALS
Article
Cite This: Chem. Mater. XXXX, XXX, XXX−XXX
pubs.acs.org/cm

Structures of $(4\text{-}Y\text{-}C_6H_4CH_2NH_3)_2PbI_4$ {Y = H, F, Cl, Br, I}: Tuning of Hybrid Organic Inorganic Perovskite Structures from Ruddlesden−Popper to Dion−Jacobson Limits

Marie-Hélène Tremblay,[†] John Bacsa,[‡] Boqin Zhao,[†,§] Federico Pulvirenti,[†] Stephen Barlow, and Seth R. Marder*,[†]

[†]Center for Organic Photonics and Electronics (COPE), School of Chemistry and Biochemistry, Georgia Institute of Technology, Atlanta, Georgia 30332-0400, United States
[‡]Crystallography Lab, Emory University, 201 Dowman Drive, Atlanta, Georgia 30322, United States

Supporting Information

ABSTRACT: In analogy to their oxide counterparts, two-dimensional (2D) hybrid organic−inorganic perovskites have been classified, in many cases, as either Dion−Jacobson (DJ) or Ruddlesden−Popper (RP) structures. We quantified the offset of the inorganic layers to allow the structures of hybrid organic inorganic perovskite to be consistently related to these two structure types. We report the structures of a family of 2D hybrid structures, $(4\text{-}Y\text{-}C_6H_4CH_2NH_3)_2PbI_4$ (where Y = F, Cl, Br, I), which consist of single ⟨100⟩-terminated perovskite sheets separated by *p*-halobenzylammonium cations. In contrast to the previous RP structure of $(C_6H_5CH_2NH_3)_2PbI_4$, where the inorganic layers are offset from each other, the Y = F, Cl, and Br examples tend toward the DJ structure, in which successive layers eclipse each other, despite the use of an organic monocation. Close Y···I approaches suggest that halogen bonding plays a role in these structures. Use of Y = I, for which stronger halogen bonding is expected and is also suggested by a more linear C−Y···I angle, results in an RP-like structure. The stability of the $(4\text{-}Y\text{-}C_6H_4CH_2NH_3)_2PbI_4$ derivatives under ambient conditions is substantially higher for Y = Br and I than for Y = H, F, and Cl.

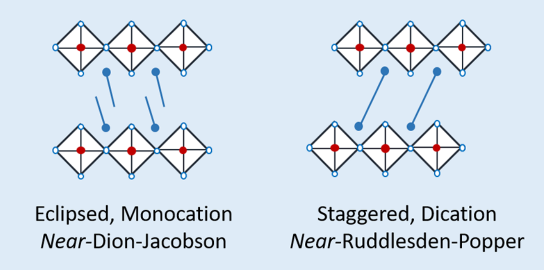

INTRODUCTION

Three-dimensional (3D) hybrid organic−inorganic perovskites (HOIPs), $BPbX_3$ (B = small organic cation; X = halide) have attracted much interest, since they have already shown promising properties in a broad variety of optoelectronic devices.[1−8] Two-dimensional (2D) HOIPs in which each planar ("(100)-oriented") layer of corner-sharing PbX_6 octahedra is separated by a layer of larger organic monocations or dications (A or A′, respectively), resulting in compositions of formula A_2PbX_4 or $A'PbX_4$, (along with so-called "quasi-2D" structures of formula $A_2B_{n-1}Pb_nX_{3n+1}$ or $A'B_{n-1}Pb_nX_{3n+1}$) have also been examined as electroactive layers in solar cells[9−18] and light-emitting diodes,[19,20] and they show higher stability then their 3D analogues, coupled with modest performance. Many other aspects of these materials have also been investigated.[21−27] The choice of the A cation or the A′ dication strongly influences the final structure of the HOIP. Multiple examples of cation−cation interactions (steric,[28−30] aromatic−aromatic,[31] van der Waals,[32] hydrogen bonding[29,33,34]) or cation-halide interactions (hydrogen bonding[35,36] halogen bonding,[37] nitro-halide interaction[31]) have been reported in materials of this type and presumably help direct the structure.

Layered oxide perovskites have been classified into different families, notably the Ruddlesden−Popper (RP) and Dion−Jacobson (DJ) structures.[38,39] *n* = 1 RP perovskites have the formula A''_2MO_4 (M = hexacoordinated ion, A′′ = interlayer metal ion). Repulsion between the two layers of A′′ cations present between each layer of MO_6 octahedra leads to an offset of one layer of MO_6 octahedra from the next by one-half of a M-to-M repeat distance in both of the M-O-M directions; this is often referenced to as a $(^1/_2, {}^1/_2)$ offset. On the other hand, DJ oxides exhibit perfect stacking with no offset between successive layers (0, 0), or a displacement of $(^1/_2, 0)$ (i.e., a shift of half a M-to-M repeat distance in one of the two M-O-M directions). This can be attributed to the single layer of ions between each layer of octahedra found in these structures; the general formula is $A'''MO_4$.

Despite the very different interlayer ion sizes and shapes used in HOIPs, their structures have often been classified in a similar way, i.e., as either as RP or DJ structures. A large number of HOIPs incorporating organic monocations—the formulas of which parallel those of RP oxides—have staggered, RP-like structures (although others have been described as "RP", apparently without consideration of the stacking motif). This can be rationalized if one assumes that the organic monocation consists of a charge-bearing headgroup (usually an

Received: April 24, 2019
Revised: August 1, 2019

DOI: 10.1021/acs.chemmater.9b01564
Chem. Mater. XXXX, XXX, XXX−XXX

ammonium group) that interacts with the inorganic layer (electrostatically and/or through hydrogen bonding) and a relatively rigid tail perpendicular to the layer; staggering the layers allows the most efficient packing of the tail groups (Figure 1). On the other hand, a dication in which two head groups are separated by a rigid bridge would be expected to hold adjacent inorganic layers in registry with each other (Figure 1). Indeed, several HOIPs with $A'PbX_4$ formulas that parallel those of $n = 1$ DJ oxides have been found to exhibit offsets typical of that class. However, the organic A and A′ monocations and dications used in HOIPs do *not* generally have rigid tails or bridges held perpendicular to the layers; in view of their irregular shapes and/or conformational flexibility, and the wealth of possible cation−cation and cation−inorganic interactions possible, it is perhaps surprising that so many examples of HOIPs appear to exhibit offsets similar to the ideal expectations for oxides with analogous formulas.

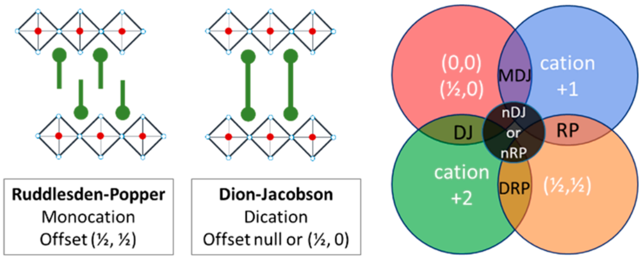

Figure 1. (Left) Schematic representation of a Ruddlesden−Popper (RP) and a Dion−Jacobson (DJ) $n = 1$ layered HOIP. (Right) Schematic representation of the different possibilities when mixing different offsets and different cations. [Legend: MDJ = monocation-DJ, DRP = dication-RP, nDJ = near-DJ ($x < {}^{1}/_{4}$, $y < {}^{1}/_{4}$), and nRP = near-RP ($x > {}^{1}/_{4}$, $y > {}^{1}/_{4}$).]

Here, we report the structures of a family of 2D HOIPs, $(Y\text{-}PMA)_2PbI_4$ ($Y\text{-}PMA = 4\text{-}Y\text{-}C_6H_4CH_2NH_3$; Y = H, F, Cl, Br, I). Despite the presence of A-site monocations, and, therefore, RP-like formulas, adjacent layers of the F, Cl, and Br examples more closely approach DJ-type stacking; we describe this class of compounds, in which the chemical formula of a RP perovskite is combined with DJ-like stacking, as monocationic-near-DJ (MnDJ) structures. In contrast, the Y = I analogue has a near-RP structure. We also classify several structures from the literature in a similar manner. In addition, we describe the cation−inorganic and cation−cation interactions in the crystals, the distortions found in the inorganic layers, and the optical and stability characteristics of the materials.

■ EXPERIMENTAL SECTION

General Method of Synthesis of Bulk Crystalline $(Y\text{-}PMA)_2PbI_4$. PbI_2 (1 equiv) was dissolved in HI (57 wt % aqueous solution) and stirred at 100 °C for 2 min. A solution of Y-PMA (2 equiv) in HI and MeOH was added to the hot PbI_2 solution, and the resultant mixture was stirred at 130 °C for 2 min. The solution was then allowed to crystallize at room temperature for 12 h. The solids were filtered and dried under high vacuum. Small peaks were often obtained at low angle, close to that at which the (00l) peaks are observed (see Figure S2 in the Supporting Information). This minor impurity did not affect the elemental analysis of the products.

Bis(phenylmethylammonium) Tetraiodoplumbate, $(PMA)_2PbI_4$. The combination of PbI_2 (129 mg, 0.28 mmol) in HI (1 mL), PMA (238 mg, 2.23 mmol) in HI (1 mL), and MeOH (0.2 mL) gave dark orange crystals (90 mg, 35%). Anal. Calcd for $(C_7H_9N)_2PbI_4$: C, 18.06%; H, 2.17%; N, 3.01%. Found: C, 18.01%; H 1.98%; N, 3.00%.

Bis(4-fluorophenylmethylammonium) Tetraiodoplumbate, $(F\text{-}PMA)_2PbI_4$. The combination of PbI_2 (131 mg, 0.28 mmol) in HI (1 mL), F-PMA (65 mg, 0.52 mmol) in HI (1 mL), and MeOH (0.8 mL) gave dark orange crystals (82 mg, 30%). Anal. Calcd for $(C_7H_9NF)_2PbI_4$: C, 17.39%; H, 1.88%; N, 2.90%. Found: C, 17.34%; H 1.75%; N, 2.96%.

Bis(4-chlorophenylmethylammonium) Tetraiodoplumbate, $(Cl\text{-}PMA)_2PbI_4$. The combination of PbI_2 (124 mg, 0.28 mmol) in HI (2 mL), Cl-PMA (78 mg, 0.55 mmol) in HI (2 mL), and MeOH (1.2 mL) gave orange crystals (96 mg, 29%). Anal. Calcd for $(C_7H_9NCl)_2PbI_4$: C, 16.81%; H, 1.81%; N, 2.80%. Found: C, 16.80%; H 1.67%; N, 2.82%.

Bis(4-bromophenylmethylammonium) Tetraiodoplumbate, $(Br\text{-}PMA)_2PbI_4$. The combination of PbI_2 (127 mg, 0.28 mmol) in HI (2 mL), PMA (103 mg, 0.55 mmol) in HI (2 mL), and MeOH (1.2 mL) gave orange crystals (135 mg, 55%). Anal. Calcd for $(C_7H_9NBr)_2PbI_4$: C, 15.44%; H, 1.67%; N, 2.57%. Found: C, 15.42%; H 1.57%; N, 2.59%.

Bis(4-iodophenylmethylammonium) Tetraiodoplumbate, $(I\text{-}PMA)_2PbI_4$. The combination of PbI_2 (202 mg, 0.45 mmol) in HI (4 mL), I-PMA (197 mg, 0.73 mmol) in HI (0.3 mL), and MeOH (4 mL) gave orange crystals (302 mg, 44%). Anal. Calcd for $(C_7H_9NI)_2PbI_4$: C, 14.21%; H, 1.53%; N, 2.37%. Found: C, 14.46%; H 1.54%; N, 2.38%.

General Method for Growth of $(Y\text{-}PMA)_2PbI_4$Single Crystals. PbI_2 in HI (1 mL of a 25 mg mL^{-1} solution) was added to a vial. MeOH (2 mL) was added on top. Y-PMA then was dissolved in a minimum of MeOH and added slowly into the vial. Orange crystals typically started to appear at the interface between the HI and MeOH after 24 h.

General Method for Obtaining $(Y\text{-}PMA)_2PbI_4$ Thin Films. A solution made by dissolving $(Y\text{-}PMA)_2PbI_4$ (10 mg) in DMF (100 μL) was spin-coated at 4000 rpm for 45 s onto a clean glass or sapphire substrate, precleaned using ultaviolet-treated ozone (UV-ozone), in a N_2-filled glovebox. Films were annealed for 30 min at 100 °C.

Single-Crystal X-ray Diffraction. Suitable crystals (see Figure S1 in the Supporting Information) were selected from the reaction mixtures obtained using the general procedure above and were mounted on a loop with paratone oil on a XtaLAB Synergy-S, Dualflex, HyPix diffractometer. Most crystals were heated to 100 K during data collection. However, crystals of $(Cl\text{-}PMA)_2PbI_4$ were found to undergo a phase transition upon cooling, with a loss of crystallinity being observed at <215 K; therefore, the crystal was cooled to 225 K during the data collection. Using OLEX2,[40] the structure was solved with the ShelXT[41] structure solution program using intrinsic phasing and refined with the ShelXL[42] refinement package using least-squares minimization. Details of the crystals, data collection, and data refinements are summarized in Table S1 in the Supporting Information. Simulated powder patterns were calculated by Mercury software, using the single-crystal X-ray CIF data.[43]

Powder X-ray Diffraction (PXRD). PXRD patterns (see Figures S2 and S3 in the Supporting Information) were acquired on a Panalytical XPert PRO Alpha-1 XRD diffractometer, using Cu K X-ray tube radiation at a voltage of 45 kV and 40 mA, with an incident beam Johannsson monochromator and an X′Celerator solid-state detector. The diffraction pattern was scanned over the angular range of 3°−40° with a step size of 0.016°, at room temperature.

Thermal Studies. The thermal behavior of the HOIPs was examined by differential scanning calorimetry using a Mettler Toledo Instrument (DSC 3+ Star system), with heating and cooling rates of 10 °C min^{-1} and a nitrogen gas flow of 80 mL min^{-1} (see Figure S4 in the Supporting Information), and by thermogravimetric analyses on a Pyris 1 TGA (Perkin−Elmer) at a heating rate of 5 °C min^{-1} under a nitrogen atmosphere (see Figure S5 in the Supporting Information for data).

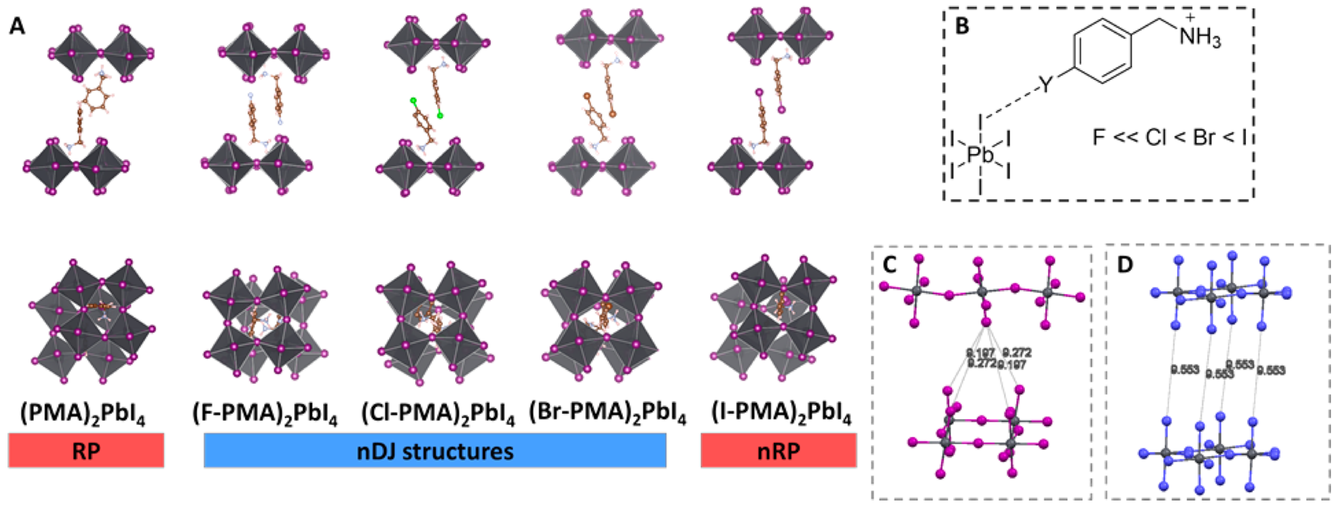

Figure 2. (A) Crystal structures of $(Y\text{-PMA})_2PbI_4$ (data for Y = H taken from ref 44): (top) side view parallel to the inorganic layers (along the short axis) and (bottom) view along an axis perpendicular to the inorganic planes. (B) Schematic representation of the halogen bonding between the iodine of the inorganic sheet and the cation. (C and D) Representations of the inorganic sheets for $(PMA)_2PbI_4$ (panel (C)) and $(Br\text{-}PMA)_2PbI_4$ (panel (D)) (cations have been removed for the sake of clarity).

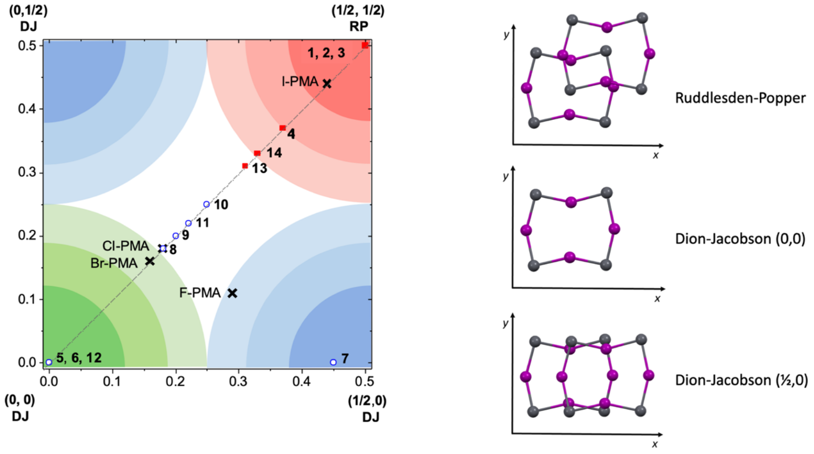

Figure 3. Left: Quantification of the offset of the two inorganic layers on the x- and y-axes for some literature A_2PbX_4 and $A'PbX_4$ HOIPs, and for the $(Y\text{-PMA})_2PbI_4$ HOIPs for which structures are reported in this work. The diagonal line indicates cases where $x = y$. The cross symbols (×) represent the new structures from this report, the open blue circles represent structures with DJ or nDJ stacking, and the solid red squares represent structures with RP or nRP stacking. The image on the right is a schematic showing that offsets of $(^1/_2, ^1/_2)$ are found for ideal RP structures and (0, 0) or $(^1/_2, 0)$ ideal DJ structures (purple = halide ions, gray = Pb ions).

RESULTS AND DISCUSSION

Synthesis. The HOIPs were synthesized using a 1:2 ratio of PbI_2 and Y-PMA iodide (where Y = F, Cl, Br, I) in a mixture of methanol and hydroiodic acid. Crystallization afforded the 2D HOIPs as bright to dark orange plates. The crystals were analyzed directly to obtain their single-crystal structures (see Figures 2, 3, and 4 where they are compared to the previously reported structure of their Y = H analogue;[44] see Figure S1 and Tables S1 and S2 in the Supporting Information) or filtered, ground, and analyzed by powder X-ray diffraction (PXRD) (see Figure S2 in the Supporting Information). The single-crystal structural data was acquired at 100 K, except in the case of $(Cl\text{-}PMA)_2PbI_4$, where this was precluded by a phase transition at ca. 175 K and where a temperature of 225 K was used instead.

All the crystals were stable in the presence of the solution from which they were grown over several days, except those based on Cl-PMA, which decomposed on a time scale of ca. 48 h. Films of the HOIPs were obtained through spin-coating onto glass substrates from dimethylformamide. All reflections seen in the Bragg-geometry PXRD patterns of the films can be indexed as (00l) reflections, corresponding to the layer stacking direction and indicating a strong preferential growth in the (001) plane to form platelike crystallites, that then lie parallel to the substrate. This is consistent with numerous previous studies of n = 1 RP and DJ systems, indicating that the orientation of the layers parallel to the substrate is strongly favored over the perpendicular one.[17] The films were used to study the stability of the materials (see Figure S3 in the Supporting Information). Ambient stability of the films in darkness was tested and analyzed using PXRD. After 1 week under ambient conditions (ca. 50% humidity, ca. 20 °C) in darkness, PbI_2 peaks were prominent and the HOIP Bragg peaks almost disappeared for films of the Y = H, F, and Cl derivatives. On the other hand, the Br- and I-analogues were unchanged, showing an increased stability for these two compounds, perhaps because of halogen-bonding interactions

DOI: 10.1021/acs.chemmater.9b01564
Chem. Mater. XXXX, XXX, XXX−XXX

(vide infra) between the heavier halogens and the iodide ions.[45] This may be related to a slight increase in hydrophobicity, as measured by the water contact angle, in the order of Y = F < Cl < Br < I (see Figure S6 in the Supporting Information).

Interlayer Stacking. In the previously reported structure of $(PMA)_2PbI_4$, in which the Y = H unsusbtituted phenylmethylammonium (benzylammonium) cation is employed, a RP structure, with perfectly offset ($^1/_2$, $^1/_2$) layers is obtained. In the present structures where the *para* position of the phenyl ring is substituted with F, Cl, or Br, the layers more closely approach DJ-type stacking (MnDJ) (see Figure 2), while the I-PMA derivative again has RP-like layer offsets (nRP). In Figure 3, we have quantified the offsets of adjacent inorganic layers as (x, y), where these coordinates correspond to the mean translation of the offsets of the Pb atoms in one plane, relative to that in the next along the two Pb−I−Pb directions (which do not necessarily correspond to the crystallographic axes), expressed as fractions of the Pb−I−Pb repeat distances.

Offset data for several previously reported structures are plotted, along with those for the present $(Y\text{-}PMA)_2PbI_4$ structures. In addition to $(PMA)_2PbI_4$, the monocations (*p*-tolylmethylammonium)$_2$PbI$_4$ (**1**),[46] (thien-2-ylmethylammonium)$_2$PbI$_4$ (**2**),[46] (cyclopropylammonium)$_2$PbI$_4$ (**3**),[47] have an "ideal" RP offset of ($^1/_2$, $^1/_2$). $(PEA)_2PbI_4$ (**4**, PEA = phenylethylammonium)[48] deviates significantly from the ideal with an offset of (0.37, 037) and therefore can be regarded as nRP. Two previously reported dication structures—(naphthalene-1,5-diyl ammonium)PbI$_4$ (**5**)[49] and (4-(ammoniomethyl)piperidinium)PbI$_4$ (**6**)[16]—are "ideal" DJ structures with translations of precisely (0, 0). Another reported dication structure, (4-(2-ammonioethyl)-1H-imidazolium)PbBr$_4$ (**7**),[50] is close to the ($^1/_2$, 0) DJ limit, with a translation of (0.42, 0), and therefore is best described as having "near-DJ" (nDJ) stacking. Another dication structure, (3-(ammoniomethyl)piperidinium)PbI$_4$ (**8**),[16] deviates more significantly from the "ideal" DJ values, but its translation of (0.18, 0.18) is still closer to one of the ideal DJ values than the RP limit and can therefore also be regarded as nDJ. Figure 3 shows that the offset for $(F\text{-}PMA)_2PbI_4$ is not particularly close to any of the ideal values; however, it is closest to the ($^1/_2$, 0) DJ limit and therefore is best considered to be a nDJ structure. $(Y\text{-}PMA)_2PbI_4$ (Y = Cl, Br) are also nDJ structures, but more closely approach the (0, 0) than the ($^1/_2$, 0) extreme and exhibit offsets similar to that seen for (3-(ammoniomethyl)piperidinium)PbI$_4$. Given that $(Y\text{-}PMA)_2PbI_4$ (Y = F, Cl, Br) incorporate organic monocations, resulting in a RP-like formula, but DJ-like layer offsets, we classify these materials as monocationic near-DJ (MnDJ) structures. A search of the literature revealed several 2D HOIPs that can also be classified as MnDJ structures, although the DJ-like aspects of their structures were not commented upon in the original publications. The offsets calculated for the structures of (2-hydroxyethylammonium)$_2$PbI$_4$ (**9**),[51] (octylammonium)$_2$PbI$_4$ (**10**),[52] and (3-bromopyridinium)$_2$PbI$_4$ (**11**),[53] are shown in Figure 3. We also found one example of a *perfect* MDJ: (5-iodopentylammonium)$_2$PbI$_4$ (**12**).[51] Finally, the translation seen for $(I\text{-}PMA)_2PbI_4$ is close to, but falls slightly short of, the ideal RP value of ($^1/_2$, $^1/_2$) and this structure can, therefore, be classified as near-RP (nRP). Again, our search of the literature revealed several 2D HOIPs that can be classified as nRP structures, such as (2-cyanoethylammonium)$_2$PbI$_4$ (**13**)[54] and (pentylammonium)$_2$PbI$_4$ (**14**).[55]

Organic−Inorganic Interactions. For the four $(Y\text{-}PMA)_2PbI_4$ compounds presented in this work, along with the previously reported structure of $(PMA)_2PbI_4$[44] and in common with the structure of many other 2D HOIPs, there is hydrogen bonding between the inorganic I^- ions and the ammonium groups. While the "head" of each cation, the ammonium moiety, is directed toward the inorganic sheet, the orientation of the tail is governed by the balance of "tail−tail" and, in some cases, "tail−inorganic" interactions that are possible. "Tail−inorganic" interactions for A_2PbX_4 HOIPs are relatively scarce. Indeed, in many such structures, including those of $(Y\text{-}PEA)_2PbI_4$ (Y-PEA = 2-(4-halophenyl)-ethylammonium, where Y = F, Cl, Br),[56] which contain A-site cations differing from the Y-PMA cations used in this work by an extra CH_2 group, the organic cations are arranged in bilayers between successive inorganic layers, and, thus, do not form head-to-tail bridges between the PbI_4 sheets. In the present series, however, there are hydrogen bonds from the NH_3^+ group of the cation to one PbI_4 sheet *and* a close approach (see Table 1) between the organic halo-substituent (Y) of the same cation and an I^- ion of the next PbI_4 sheets; in some cases, this approach may reflect a halogen bonding interaction in which Y is the halogen-bond donor (Lewis acid) and I^- the acceptor (Lewis base). In the case of $(PMA)_2PbI_4$, the H···I distance exceeds the sum of the van der Waals radii (from refs 57 and 58) and therefore likely does not represent a significant interaction. In the case of $(F\text{-}PMA)_2PbI_4$, one of two inequivalent Y···I distances is close to the sum of van der Waals radii, but the corresponding C−F···I angle is far from the ideal 180° expected for a halogen bond. In this case, a hydrogen bonding interaction between the F atom and the NH_3^+ group of a neighboring cation may be responsible for the close F···I approach. In the case of $(Cl\text{-}PMA)_2PbI_4$, the Cl···I distances are both somewhat larger than the sum of the van der Waals radii, but both C−Cl···I interactions are more linear than the short contact seen for Y = F, with the shortest of the two being the more linear. For $(Br\text{-}PMA)_2PbI_4$ and $(I\text{-}PMA)_2PbI_4$, the Y···I contacts are similar to or shorter than van der Waals contacts. The C−Br···I angles are similar to the C−Cl···I angles, while the C−I···I interaction is the most linear of any of the C−Y···I interactions seen here. The tendency toward shorter (relative to van der Waals radii) and more linear interactions seen for the heavier halogens is consistent with the strength of C−Y bonds as halogen bond donors, which increases in the order of F < Cl < Br < I (see Figure 4).[59]

Table 1. Selected Distances and Angles in the Crystal Structures of $(Y\text{-}PMA)_2PbI_4$

Y	I···Y distance (Å)	sum of Y and I VdW radii[a] (Å)	I···Y−C_4 angle (deg)	interlayer I···I distance (Å)
H[b]	3.488	3.07	140.78	9.197
F	3.478, 3.954	3.45	118.7, 157.2	7.777
Cl	4.039, 3.933	3.73	146.41, 164.49	9.546
Br	3.894, 3.805	3.83	150.67, 164.49	9.553
I	3.931	3.96	168.2	10.771

[a] van der Waals radii for halogens and hydrogen were taken from refs 57 and 58, respectively. [b] Data taken from ref 44.

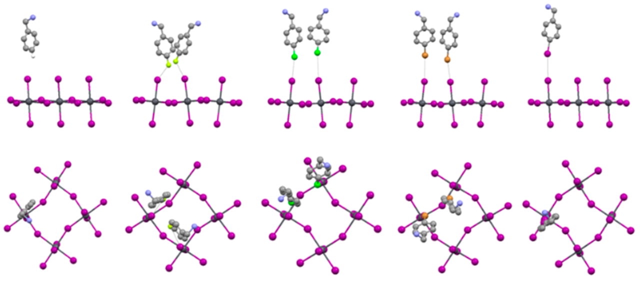

Figure 4. Representation of the possible close Y···I approaches between the halo substituent of the organic cation and the inorganic sheet of $(Y\text{-}PMA)_2PbI_4$ (from left to right, Y = H, F, Cl, Br, and I). Note that for Y = F, Cl, and Br, there are two inequivalent cations in the asymmetric unit, whereas there is only one for Y = H and I.

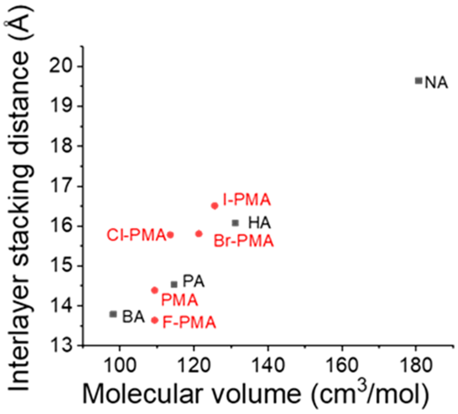

Figure 5. (A) Relationship between the interlayer stacking distance and the molar volume for alkylammonium HOIPs (black squares) and for $(Y\text{-}PMA)_2PbI_4$ derivatives (red circles). The interlayer stacking distance is extracted from the reported crystal structure of butylammonium (BA),[60] pentylammonium (PA),[55] hexylammonium (HA),[55] and nonylammomium (NA).[52]

Figure 5 shows a related observation. For 2D HOIPs incorporating increasingly large cations of similar structure, a linear trend is often observed between the interlayer stacking distance and molecular volume of the cation (see black squares for the alkylammonium series in Figure 5). In the present series, the trend is not observed (see red circles in Figure 5); in particular, the Cl- and Br-PMA derivatives show very similar interlayer spacings, despite an increase in cation volume of 7.7 $cm^3\ mol^{-1}$. This can be attributed to the counterbalancing of the increased molecular volume by stronger halogen bonding in the Br-PMA derivative, which results in Br···I contacts that are shorter than the Cl···I distances.

However, despite the evidence for halogen bonding in some of these structures, $(Br\text{-}PMA)_2PbI_4$ and $(I\text{-}PMA)_2PbI_4$, in which the strongest halogen bonding is both suggested by the crystallographic data and expected based on theoretical considerations, exhibit very different structures, notably exhibiting nDJ and nRP offsets, respectively. In contrast, $(Cl\text{-}PMA)_2PbI_4$ and $(Br\text{-}PMA)_2PbI_4$ adopt similar packing and nDJ translations, despite their different halogen-bonding strengths. Thus, although halogen bonding allows the Y-PMA monocations to act as interlayer bridges, potentially affecting the stacking of the inorganic layers, the conformational flexibility of the cations, combined with the other cation−cation interactions present, steric hindrance, and the various distortions of the PbI_4 layers that can occur, means that halogen bonding is not the only factor. Interestingly, while the present series shows an evolution from RP to MnDJ to nRP with increasing halogen size and potential halogen-bonding strength, a series of $(CH_3(CH_2)_{m-1}NH_3)_2PbI_4$ structures,[52,55,60,61] with m = 4−10, 12, 14, 16, 18 (the m = 2 and 3 cations lead to compounds containing one-dimensional (1D) chains of face-sharing octahedra of formula $APbI_3$, rather than 2D HOIPs[62,63]) shows a similar evolution from ideal RP (m = 4) to near-ideal MnDJ (m = 6) and back to ideal RP (m = 10+) with increasing alkyl chain length and increasing alkyl−alkyl van der Waals interaction (see Figure S7 in the Supporting Information). Even in the $(Y\text{-}PEA)_2PbI_4$ series (Y = H, F, Cl, Br),[48,56] where there is a bilayer of organic cations, but in which the cation−cation interaction strength likely increases with the halogen polarizability, the deviation from ideal RP stacking increases from Y = H to Y = F, with ideal RP stacking for Y = Cl, and Br (see Figure S7).

Cation−cation interactions and contacts in the $(Y\text{-}PMA)_2PbI_4$ structures are shown in Figure S8 in the Supporting Information. As noted above, C−Y···H hydrogen bonding is present in some structures. Another interesting feature is the presence of π−π interactions between F-PMA cations; this is a rare interaction for HOIPs, with only a few examples given in the literature.[31] The distortions in the inorganic portion of the structures are discussed in the following section.

Distortions within the PbI_4 Layers. Various distortions have been found in the PbX_4 layers of HOIPs and, in various series of compounds, have been correlated with optical properties. One important structural parameter that can be

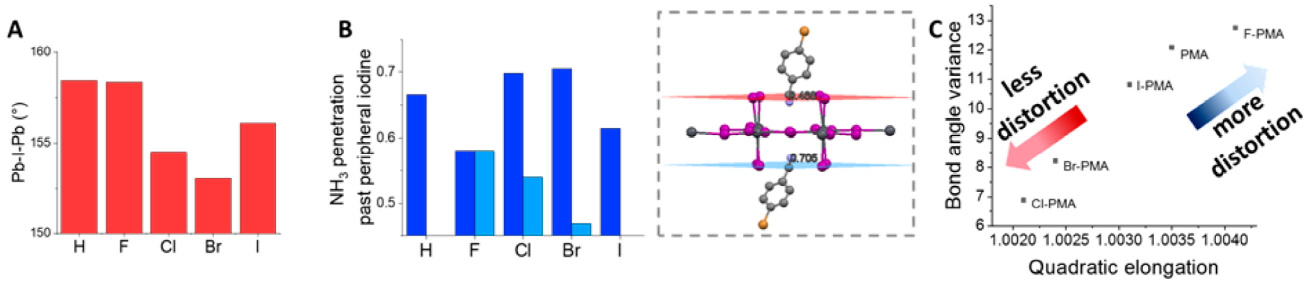

Figure 6. Comparisons of (A) the Pb−I−Pb angles and (B) the ammonium penetration past the peripheral iodine for $(Y\text{-}PMA)_2PbI_4$ (where Y = H, F, Cl, Br, I). The ammonium penetration is the distance between the nitrogen of the ammonium and the plane made by the four iodine of the octahedron. Because of the crystallographic symmetry of the crystal structures, there are two values for the Cl and Br compounds. (C) Relationship between the bond angle variance and the quadratic elongation.

used to describe HOIPs is the Pb–I–Pb angle (see Figure 6A and Table 2), where larger Pb–I–Pb angles represent less distortion; smaller distortions have been correlated with lower exciton energy for both RP and DJ perovskites.[64] In the series presented here, these distortions are fairly large, and fall into a relative narrow range of 150°–160°. The Br-PMA compound has the smallest Pb–I–Pb angle (151°), while its F- and H-analogues have the largest (ca. 158°). The ammonium penetration past the peripheral iodine is also related to the Pb–I–Pb angle.[48] As mentioned previously, the $(Cl\text{-}PMA)_2PbI_4$ and $(Br\text{-}PMA)_2PbI_4$ structures are less symmetric than the Y = H and Y = I analogues, perhaps due to the asymmetrical ammonium penetration (see Figure 6B). $(F\text{-}PMA)_2PbI_4$ is also slightly asymmetrical. Because of the large penetration on one side, the octahedra tilt away from each other on that side, which results in a tilt toward each other on the opposite face of the PbI_4 layer, allowing only a small penetration of the other ammonium. In this series, as the ammonium penetration is increased (taking, where relevant, the largest of the two values), the Pb–I–Pb angle is reduced, showing more distortion.

Table 2. Distortion Parameters for the PbI_4 Layers in the Crystal Structures of $(Y\text{-}PMA)_2PbI_4$[a]

Y	Pb–I–Pb (deg)	r(Pb–I),avg (Å)	λ_{oct}	σ_{oct}^2 (deg^2)
H[b]	158.43	3.2082	1.0035	12.0819
F	158.00, 158.69	3.2090	1.0041	12.7554
Cl	153.91, 155.07	3.1907	1.0021	6.8871
Br	151.34, 154.75	3.1868	1.0024	8.2175
I	156.11	3.1840	1.0031	10.8138

[a] Calculated using VESTA.[65] [b] Data taken from ref 44.

The distortion of the geometry of the PbI_6 octahedra from regularity has also been discussed in the literature and correlated with optical properties. This distortion can be gauged through the quadratic elongation (λ_{oct}) or the bond angle variance (σ^2_{oct}):[66]

$$\lambda_{oct} = \frac{1}{6}\sum_{i=1}^{6}\left(\frac{d_i}{d_0}\right)^2 \tag{1}$$

$$\sigma_{oct}^2 = \frac{1}{11}\sum_{i=1}^{12}(\alpha_i - 90)^2 \tag{2}$$

where d_i is the Pb–I bond length, d_0 the center-to-vertex distance of a regular polyhedron of the same volume, and α_i the I–Pb–I angle. In the present series, there is good correlation between the two measures of distortion (Figure 6C), consistent with that seen for most other haloplumbate HOIPs.[66] However, the distortions are all relatively small and there is no obvious trend with the identity of Y (see Table 2 and Figure 6C). We recently demonstrated that the ^{207}Pb NMR chemical shift ($\delta(^{207}Pb)$) for planar and corrugated A_2PbI_4 and $A'PbI_4$ compounds correlates linearly with λ_{oct}. As shown in Figure S9 in the Supporting Information, data for $(Br\text{-}PMA)_2PbI_4$ also fit this relation.

Optical Properties. The photophysical properties of the HOIP films and powders (the PXRD patterns of which were, in each case, consistent with those calculated using the relevant single-crystal parameters, as shown in Figure S2) were investigated by UV-vis absorption (films) or diffuse reflectance (powders) spectroscopy and steady-state photoluminescence (PL) spectroscopy[67] (see Figure 7 and Table 3 for film data; data for powders are shown in Figure S10 in the Supporting Information).

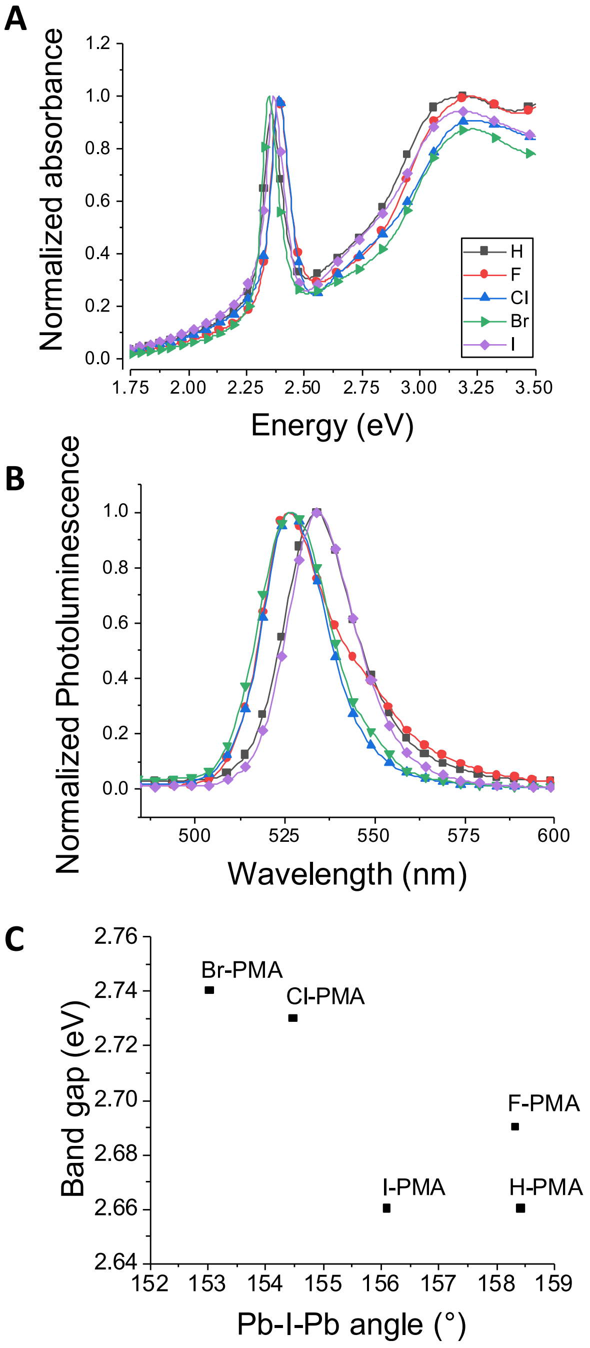

Figure 7. (A) Absorption and (B) PL spectra of the HOIP films. (C) Relationship between the band gap and the average Pb–I–Pb angle.

Table 3. Optical Properties of $(Y\text{-}PMA)_2PbI_4$ Films

Y	E_g (eV)	E_{ex} (eV)	photoluminescence, PL (eV)	color
H	2.66	2.29	2.32	dark orange
F	2.69	2.33	2.36	dark orange
Cl	2.73	2.33	2.36	pale orange
Br	2.74	2.28	2.36	pale orange
I	2.66	2.29	2.32	dark orange

The exciton energy (E_{ex}) is estimated by extrapolating the low-energy edge of the low-energy discrete peak in the UV-vis absorption spectra to the energy axis, while the bandgap (E_g) is estimated by extrapolating the edge of the higher-energy feature to the energy axis. Overall, there is relatively little variation in the energies in the present series. As shown in Figure 7C, values of E_g (but not of E_{ex} or the PL) correlate fairly well with the Pb–I–Pb angle over the series, which is a relationship that has previously been suggested;[64] the deviations from this relationship may be due to the competing effects of other structural features, but it should be emphasized that the ranges of Pb–I–Pb angles and E_g values are both relatively small, compared to those seen in ref 64 Regardless, the Cl-PMA and Br-PMA derivatives, which exhibit the smallest (most distorted) Pb–I–Pb angles of this series *do* exhibit the highest values of E_g. The values of E_g also show some correlation with λ_{oct} and σ_{oct}^2 (see Figure S11 in the Supporting Information). The PL spectrum for $(F\text{-PMA})_2PbI_4$ is the broadest one among those collected (Figure 7B), following the expected trend where the structure with the most distorted octahedra, as measured by the quadratic elongation, has a larger full-width at half-maximum (fwhm).

Note that some DJ $A'PbI_4$ structures have been previously found to exhibit lower band gaps than typical RP HOIPs. However, this is attributed to closer I···I interlayer distances (arising from relatively small bridging dications) and to less distorted inorganic frameworks, rather than being a direct consequence of the different stacking motifs.[16] In the present series, the *largest* band gaps are found for the MnDJ structures (Y = F, Cl, Br). However, the interlayer distances in the present MnDJ structures are much greater than those in previously studied DJ examples (and, as shown in Figure 5, there is no clear pattern in this distance between (n)RP and MnDJ structure types), and they are likely sufficiently large to preclude the layer–layer interactions thought to be responsible for the red-shift of previous DJ examples. In addition, two of the MnDJ structures (Y = Cl, Br) exhibit the most distorted Pb–I–Pb angles and least distorted octahedra, while the other nDJ structure (Y = F) has the least-distorted Pb–I–Pb angles and most distorted octahedra.

CONCLUSION

In summary, we have reported the structures, optical properties, film formation, and stability data of a series of A_2PbI_4 HOIPs employing Y-PMA cations, where Y = F, Cl, Br, and I, and compared them to those of their Y = H analogue. Short contacts are seen between the halo substituents of the cations and the iodides of the inorganic sheets; in particular, the Y···I distances and C–Y···I geometries seen for Y = Br and I are suggestive of halogen bonding. Moreover, we have quantified the DJ- vs RP-like nature of 2D HOIPs, according to the offsets of subsequent inorganic layers; this may prove useful in classifying other HOIPs. We classify the Y = F, Cl, and Br derivatives as "MnDJ" on the basis that they include organic monocations, but exhibit stacking of the inorganic layers that is closer to that found in DJ perovskites than in RP perovskites. For the X = I example, a more RP-like stacking is observed. Examination of the literature crystal structures reveals some similar behavior in other series, suggesting that the trends in the stacking motif can perhaps be correlated with those in the strength of organic–inorganic or organic–organic interactions. Based on the stacking obtained for a given cation, it may even be possible to engineer stronger or weaker interactions in order to obtain whichever stacking pattern is desired. Further systematic structural studies of A_2PbX_4 HOIPs that contain families of closely related cations will be required to validate or refute this idea.

The distortions of the inorganic layers in the $(Y\text{-PMA})_2PbI_4$ series have also been examined; in particular, when the ammonium penetration is increased, the Pb–I–Pb angle is reduced, showing more distortion in the plane of the sheet. Further understanding of the role of cation–cation and cation-inorganic sheet interactions may help engineer new HOIPs; the findings presented here underscore the importance of increasing the library of HOIP structures, in particular of MnDJ structures, available in order to attempt to understand the factors determining their structural characteristics. The optical properties of the series show relative minor variations, consistent with the large interlayer spacings and highly distorted Pb–I–Pb angles found in each case.

ASSOCIATED CONTENT

Supporting Information

The Supporting Information is available free of charge on the ACS Publications website at DOI: 10.1021/acs.chemmater.9b01564.

- Crystallographic data for $(4\text{-F-PMA})_2PbI_4$ (CIF)
- Crystallographic data for $(4\text{-Cl-PMA})_2PbI_4$ (CIF)
- Crystallographic data for $(4\text{-Br-PMA})_2PbI_4$ (CIF)
- Tables of crystallographic data, additional figures showing structural features, ^{207}Pb SS-NMR, and stability data (PDF)
- Crystallographic data for $(4\text{-I-PMA})_2PbI_4$ (CIF)

AUTHOR INFORMATION

Corresponding Author

*E-mail: seth.marder@chemistry.gatech.edu.

ORCID

John Bacsa: 0000-0001-5681-4458
Stephen Barlow: 0000-0001-9059-9974
Seth R. Marder: 0000-0001-6921-2536

Present Address

[§]Beijing National Laboratory for Molecular Sciences, State Key Laboratory of Rare Earth Materials and Applications, College of Chemistry and Molecular Engineering, Peking University, Beijing 100871, PRC.

Notes

The authors declare no competing financial interest.

ACKNOWLEDGMENTS

This work was supported by NSERC (ES. D. Scholarship for MHT) and the AFOSR (No. FA9550-18-1-0499).

REFERENCES

(1) Kojima, A.; Teshima, K.; Shirai, Y.; Miyasaka, T. Organometal Halide Perovskites as Visible-Light Sensitizers for Photovoltaic Cells. *J. Am. Chem. Soc.* **2009**, *131*, 6050–6051.

(2) Zhou, H.; Chen, Q.; Li, G.; Luo, S.; Song, T.-b.; Duan, H.-S.; Hong, Z.; You, J.; Liu, Y.; Yang, Y. Interface Engineering of Highly Efficient Perovskite Solar Cells. *Science* **2014**, *345*, 542–546.

(3) Lee, M. M.; Teuscher, J.; Miyasaka, T.; Murakami, T. N.; Snaith, H. J. Efficient Hybrid Solar Cells Based on Meso-Superstructured Organometal Halide Perovskites. *Science* **2012**, *338*, 643–647.

(4) Arora, N.; Dar, M. I.; Hinderhofer, A.; Pellet, N.; Schreiber, F.; Zakeeruddin, S. M.; Grätzel, M. Perovskite Solar Cells with Cuscn

Hole Extraction Layers Yield Stabilized Efficiencies Greater Than 20%. *Science* **2017**, *358*, 768−771.

(5) Yang, W. S.; Park, B.-W.; Jung, E. H.; Jeon, N. J.; Kim, Y. C.; Lee, D. U.; Shin, S. S.; Seo, J.; Kim, E. K.; Noh, J. H.; Seok, S. I. Iodide Management in Formamidinium-Lead-Halide−Based Perovskite Layers for Efficient Solar Cells. *Science* **2017**, *356*, 1376−1379.

(6) Stoumpos, C. C.; Kanatzidis, M. G. Halide Perovskites: Poor Man's High-Performance Semiconductors. *Adv. Mater.* **2016**, *28*, 5778−5793.

(7) Chin, X. Y.; Cortecchia, D.; Yin, J.; Bruno, A.; Soci, C. Lead Iodide Perovskite Light-Emitting Field-Effect Transistor. *Nat. Commun.* **2015**, *6*, 7383.

(8) Zhou, B.; Jiang, M.; Dong, H.; Zheng, W.; Huang, Y.; Han, J.; Pan, A.; Zhang, L. High-Temperature Upconverted Single-Mode Lasing in 3d Fully Inorganic Perovskite Microcubic Cavity. *ACS Photonics* **2019**, *6*, 793−801.

(9) Smith, I. C.; Hoke, E. T.; Solis-Ibarra, D.; McGehee, M. D.; Karunadasa, H. I. A Layered Hybrid Perovskite Solar-Cell Absorber with Enhanced Moisture Stability. *Angew. Chem., Int. Ed.* **2014**, *53*, 11232−11235.

(10) Yan, J.; Qiu, W.; Wu, G.; Heremans, P.; Chen, H. Recent Progress in 2D/Quasi-2D Layered Metal Halide Perovskites for Solar Cells. *J. Mater. Chem. A* **2018**, *6*, 11063−11077.

(11) Chen, Y.; Sun, Y.; Peng, J.; Zhang, W.; Su, X.; Zheng, K.; Pullerits, T.; Liang, Z. Tailoring Organic Cation of 2D Air-Stable Organometal Halide Perovskites for Highly Efficient Planar Solar Cells. *Adv. Energy Mater.* **2017**, *7*, 1700162.

(12) Cao, D. H.; Stoumpos, C. C.; Farha, O. K.; Hupp, J. T.; Kanatzidis, M. G. 2D Homologous Perovskites as Light-Absorbing Materials for Solar Cell Applications. *J. Am. Chem. Soc.* **2015**, *137*, 7843−7850.

(13) Ma, C.; Shen, D.; Ng, T.-W.; Lo, M.-F.; Lee, C.-S. 2D Perovskites with Short Interlayer Distance for High-Performance Solar Cell Application. *Adv. Mater.* **2018**, *30*, 1800710.

(14) Lai, H.; Kan, B.; Liu, T.; Zheng, N.; Xie, Z.; Zhou, T.; Wan, X.; Zhang, X.; Liu, Y.; Chen, Y. Two-Dimensional Ruddlesden−Popper Perovskite with Nanorod-Like Morphology for Solar Cells with Efficiency Exceeding 15%. *J. Am. Chem. Soc.* **2018**, *140*, 11639−11646.

(15) Tsai, H.; Nie, W.; Blancon, J.-C.; Stoumpos, C. C.; Asadpour, R.; Harutyunyan, B.; Neukirch, A. J.; Verduzco, R.; Crochet, J. J.; Tretiak, S.; Pedesseau, L.; Even, J.; Alam, M. A.; Gupta, G.; Lou, J.; Ajayan, P. M.; Bedzyk, M. J.; Kanatzidis, M. G.; Mohite, A. D. High-Efficiency Two-Dimensional Ruddlesden−Popper Perovskite Solar Cells. *Nature* **2016**, *536*, 312.

(16) Mao, L.; Ke, W.; Pedesseau, L.; Wu, Y.; Katan, C.; Even, J.; Wasielewski, M. R.; Stoumpos, C. C.; Kanatzidis, M. G. Hybrid Dion−Jacobson 2D Lead Iodide Perovskites. *J. Am. Chem. Soc.* **2018**, *140*, 3775−3783.

(17) Stoumpos, C. C.; Cao, D. H.; Clark, D. J.; Young, J.; Rondinelli, J. M.; Jang, J. I.; Hupp, J. T.; Kanatzidis, M. G. Ruddlesden−Popper Hybrid Lead Iodide Perovskite 2D Homologous Semiconductors. *Chem. Mater.* **2016**, *28*, 2852−2867.

(18) Ahmad, S.; Fu, P.; Yu, S.; Yang, Q.; Liu, X.; Wang, X.; Wang, X.; Guo, X.; Li, C. Dion-Jacobson Phase 2D Layered Perovskites for Solar Cells with Ultrahigh Stability. *Joule* **2019**, *3*, 794−806.

(19) Yuan, M.; Quan, L. N.; Comin, R.; Walters, G.; Sabatini, R.; Voznyy, O.; Hoogland, S.; Zhao, Y.; Beauregard, E. M.; Kanjanaboos, P.; Lu, Z.; Kim, D. H.; Sargent, E. H. Perovskite Energy Funnels for Efficient Light-Emitting Diodes. *Nat. Nanotechnol.* **2016**, *11*, 872.

(20) Tsai, H.; Nie, W.; Blancon, J.-C.; Stoumpos, C. C.; Soe, C. M. M.; Yoo, J.; Crochet, J.; Tretiak, S.; Even, J.; Sadhanala, A.; Azzellino, G.; Brenes, R.; Ajayan, P. M.; Bulović, V.; Stranks, S. D.; Friend, R. H.; Kanatzidis, M. G.; Mohite, A. D. Stable Light-Emitting Diodes Using Phase-Pure Ruddlesden−Popper Layered Perovskites. *Adv. Mater.* **2018**, *30*, 1704217.

(21) Dou, L.; Wong, A. B.; Yu, Y.; Lai, M.; Kornienko, N.; Eaton, S. W.; Fu, A.; Bischak, C. G.; Ma, J.; Ding, T.; Ginsberg, N. S.; Wang, L.-W.; Alivisatos, A. P.; Yang, P. Atomically Thin Two-Dimensional Organic-Inorganic Hybrid Perovskites. *Science* **2015**, *349*, 1518−1521.

(22) Tian, H.; Zhao, L.; Wang, X.; Yeh, Y.-W.; Yao, N.; Rand, B. P.; Ren, T.-L. Extremely Low Operating Current Resistive Memory Based on Exfoliated 2d Perovskite Single Crystals for Neuromorphic Computing. *ACS Nano* **2017**, *11*, 12247−12256.

(23) Blancon, J.-C.; Tsai, H.; Nie, W.; Stoumpos, C. C.; Pedesseau, L.; Katan, C.; Kepenekian, M.; Soe, C. M. M.; Appavoo, K.; Sfeir, M. Y.; Tretiak, S.; Ajayan, P. M.; Kanatzidis, M. G.; Even, J.; Crochet, J. J.; Mohite, A. D. Extremely Efficient Internal Exciton Dissociation through Edge States in Layered 2D Perovskites. *Science* **2017**, *355*, 1288−1292.

(24) Wang, J.; Su, R.; Xing, J.; Bao, D.; Diederichs, C.; Liu, S.; Liew, T. C. H.; Chen, Z.; Xiong, Q. Room Temperature Coherently Coupled Exciton-Polaritons in Two-Dimensional Organic-Inorganic Perovskite. *ACS Nano* **2018**, *12*, 8382−8389.

(25) Tu, Q.; Spanopoulos, I.; Yasaei, P.; Stoumpos, C. C.; Kanatzidis, M. G.; Shekhawat, G. S.; Dravid, V. P. Stretching and Breaking of Ultrathin 2d Hybrid Organic-Inorganic Perovskites. *ACS Nano* **2018**, *12*, 10347−10354.

(26) Thouin, F.; Valverde-Chávez, D. A.; Quarti, C.; Cortecchia, D.; Bargigia, I.; Beljonne, D.; Petrozza, A.; Silva, C.; Srimath Kandada, A. R. Phonon Coherences Reveal the Polaronic Character of Excitons in Two-Dimensional Lead Halide Perovskites. *Nat. Mater.* **2019**, *18*, 349−356.

(27) Wei, W.-J.; Jiang, X.-X.; Dong, L.-Y.; Liu, W.-W.; Han, X.-B.; Qin, Y.; Li, K.; Li, W.; Lin, Z.-S.; Bu, X.-H.; Lu, P.-X. Regulating Second-Harmonic Generation by Van Der Waals Interactions in Two-Dimensional Lead Halide Perovskite Nanosheets. *J. Am. Chem. Soc.* **2019**, *141*, 9134−9139.

(28) Xu, Z.; Mitzi, D. B. SnI_4^{2-}-Based Hybrid Perovskites Templated by Multiple Organic Cations: Combining Organic Functionalities through Noncovalent Interactions. *Chem. Mater.* **2003**, *15*, 3632−3637.

(29) Yu, T.; Zhang, L.; Shen, J.; Fu, Y.; Fu, Y. Hydrogen Bonds and Steric Effects Induced Structural Modulation of Three Layered Iodoplumbate Hybrids from Nonperovskite to Perovskite Structure. *Dalton Trans* **2014**, *43*, 13115−13121.

(30) Xu, Z.; Mitzi, D. B.; Dimitrakopoulos, C. D.; Maxcy, K. R. Semiconducting Perovskites $(2\text{-}XC_6H_4C_2H_4NH_3)_2SnI_4$ (X = F, Cl, Br): Steric Interaction between the Organic and Inorganic Layers. *Inorg. Chem.* **2003**, *42*, 2031−2039.

(31) Tremblay, M.-H.; Thouin, F.; Leisen, J.; Bacsa, J.; Srimath Kandada, A. R.; Hoffman, J. M.; Kanatzidis, M. G.; Mohite, A. D.; Silva, C.; Barlow, S.; Marder, S. R. $(4NPEA)_2PbI_4$ (4NPEA = 4-Nitrophenylethylammonium): Structural, NMR, and Optical Properties of a 3 × 3 Corrugated 2D Hybrid Perovskite. *J. Am. Chem. Soc.* **2019**, *141*, 4521−4525.

(32) Yao, Z.; Zhou, Y.; Yin, X.; Li, X.; Han, J.; Tai, M.; Zhou, Y.; Li, J.; Hao, F.; Lin, H. Role of Alkyl Chain Length in Diaminoalkane Linked 2d Ruddlesden−Popper Halide Perovskites. *CrystEngComm* **2018**, *20*, 6704−6712.

(33) Mercier, N.; Poiroux, S.; Riou, A.; Batail, P. Unique Hydrogen Bonding Correlating with a Reduced Band Gap and Phase Transition in the Hybrid Perovskites $(HO(CH_2)_2NH_3)_2PbX_4$ (X = I, Br). *Inorg. Chem.* **2004**, *43*, 8361−8366.

(34) Li, J.; Yan, K.; Chen, J.; Zhang, Y.; Yang, W.; Lian, X.; Wu, G.; Chen, H. Hydrogen Bond Enables Highly Efficient and Stable Two-Dimensional Perovskite Solar Cells Based on 4-Pyridine-Ethylamine. *Org. Electron.* **2019**, *67*, 122−127.

(35) Lee, J. H.; Lee, J.-H.; Kong, E.-H.; Jang, H. M. The Nature of Hydrogen-Bonding Interaction in the Prototypic Hybrid Halide Perovskite, Tetragonal $CH_3NH_3PbI_3$. *Sci. Rep.* **2016**, *6*, 21687.

(36) El-Mellouhi, F.; Bentria, E. T.; Marzouk, A.; Rashkeev, S. N.; Kais, S.; Alharbi, F. H. Hydrogen Bonding: A Mechanism for Tuning Electronic and Optical Properties of Hybrid Organic−Inorganic Frameworks. *Npj Comput. Mater.* **2016**, *2*, 16035.

(37) Sourisseau, S.; Louvain, N.; Bi, W.; Mercier, N.; Rondeau, D.; Boucher, F.; Buzaré, J.-Y.; Legein, C. Reduced Band Gap Hybrid

Perovskites Resulting from Combined Hydrogen and Halogen Bonding at the Organic-Inorganic Interface. *Chem. Mater.* **2007**, *19*, 600−607.

(38) Lichtenberg, F.; Herrnberger, A.; Wiedenmann, K.; Mannhart, J. Synthesis of Perovskite-Related Layered $A_nB_nO_{3n+2}$ = ABO_x Type Niobates and Titanates and Study of Their Structural, Electric and Magnetic Properties. *Prog. Solid State Chem.* **2001**, *29*, 1−70.

(39) Lichtenberg, F.; Herrnberger, A.; Wiedenmann, K. Synthesis, Structural, Magnetic and Transport Properties of Layered Perovskite-Related Titanates, Niobates and Tantalates of the Type $A_nB_nO_{3n+2}$, $A'A_{k-1}B_kO_{3k+1}$ and $A_mB_{m-1}O_{3m}$. *Prog. Solid State Chem.* **2008**, *36*, 253−387.

(40) Dolomanov, O. V.; Bourhis, L. J.; Gildea, R. J.; Howard, J. A. K.; Puschmann, H. OLEX2: A Complete Structure Solution, Refinement and Analysis Program. *J. Appl. Crystallogr.* **2009**, *42*, 339−341.

(41) Sheldrick, G. M. ShelXT - Integrated Space-Group and Crystal-Structure Determination. *Acta Crystallogr., Sect. A: Found. Adv.* **2015**, *71*, 3−8.

(42) Sheldrick, G. M. Crystal Structure Refinement with ShelXL. *Acta Crystallogr., Sect. C: Struct. Chem.* **2015**, *71*, 3−8.

(43) Macrae, C. F.; Edgington, P. R.; McCabe, P.; Pidcock, E.; Shields, G. P.; Taylor, R.; Towler, M.; van de Streek, J. Mercury: Visualization and Analysis of Crystal Structures. *J. Appl. Crystallogr.* **2006**, *39*, 453−457.

(44) Papavassiliou, G. C.; Mousdis, G. A.; Raptopoulou, C. P.; Terzis, A. Preparation and Characterization of $[C_6H_5CH_2NH_3]_2PbI_4$, $[C_6H_5CH_2CH_2SC(NH_2)_2]_3PbI_5$ and $[C_{10}H_7CH_2NH_3]$ PbI_3 Organic-Inorganic Hybrid Compounds. *Z. Naturforsch., B: J. Chem. Sci.* **1999**, *54*, 1405−1409.

(45) The thermal stability of Y = H, F, Cl, and Br compounds was also investigated using thermogravimetric analysis of solid samples: all four materials only lose weight at temperatures above ca. 320 °C (see Figure S5 in the Supporting Information).

(46) Zhu, X.-H.; Mercier, N.; Riou, A.; Blanchard, P.; Frère, P. $(C_4H_3SCH_2NH_3)_2(CH_3NH_3)Pb_2I_7$: Non-Centrosymmetrical Crystal Structure of a Bilayer Hybrid Perovskite. *Chem. Commun.* **2002**, 2160−2161.

(47) Billing, D. G.; Lemmerer, A. Inorganic−Organic Hybrid Materials Incorporating Primary Cyclic Ammonium Cations: The Lead Iodide Series. *CrystEngComm* **2007**, *9*, 236−244.

(48) Du, K.-z.; Tu, Q.; Zhang, X.; Han, Q.; Liu, J.; Zauscher, S.; Mitzi, D. B. Two-Dimensional Lead(II) Halide-Based Hybrid Perovskites Templated by Acene Alkylamines: Crystal Structures, Optical Properties, and Piezoelectricity. *Inorg. Chem.* **2017**, *56*, 9291−9302.

(49) Lemmerer, A.; Billing, D. G. Lead Halide Inorganic−Organic Hybrids Incorporating Diammonium Cations. *CrystEngComm* **2012**, *14*, 1954−1966.

(50) Smith, M. D.; Jaffe, A.; Dohner, E. R.; Lindenberg, A. M.; Karunadasa, H. I. Structural Origins of Broadband Emission from Layered Pb−Br Hybrid Perovskites. *Chem. Sci.* **2017**, *8*, 4497−4504.

(51) Lemmerer, A.; Billing, D. G. Effect of Heteroatoms in the Inorganic−Organic Layered Perovskite-Type Hybrids $[(ZC_nH_{2n}NH_3)_2PbI_4]$, n = 2, 3, 4, 5, 6; Z = OH, Br and I; and $[(H_3NC_2H_4S_2C_2H_4NH_3)PbI_4]$. *CrystEngComm* **2010**, *12*, 1290−1301.

(52) Lemmerer, A.; Billing, D. G. Synthesis, Characterization and Phase Transitions of the Inorganic−Organic Layered Perovskite-Type Hybrids $[[(C_nH_{2n+1}NH_3)_2PbI_4]$, n = 7, 8, 9 and 10. *Dalton Trans* **2012**, *41*, 1146−1157.

(53) Gómez, V.; Fuhr, O.; Ruben, M. Structural Diversity in Substituted-Pyridinium Iodo- and Bromoplumbates: A Matter of Halide and Temperature. *CrystEngComm* **2016**, *18*, 8207−8219.

(54) Mercier, N.; Louvain, N.; Bi, W. Structural Diversity and Retro-Crystal Engineering Analysis of Iodometalate Hybrids. *CrystEngComm* **2009**, *11*, 720−734.

(55) Billing, D. G.; Lemmerer, A. Synthesis, Characterization and Phase Transitions in the Inorganic-Organic Layered Perovskite-Type Hybrids $[(C_nH_{2n+1}NH_3)_2PbI_4]$, n = 4, 5 and 6. *Acta Crystallogr., Sect. B: Struct. Sci.* **2007**, *63*, 735−747.

(56) Straus, D. B.; Iotov, N.; Gau, M. R.; Zhao, Q.; Carroll, P. J.; Kagan, C. R. Longer Cations Increase Energetic Disorder in Excitonic 2d Hybrid Perovskites. *J. Phys. Chem. Lett.* **2019**, *10*, 1198−1205.

(57) Rowland, R. S.; Taylor, R. Intermolecular Nonbonded Contact Distances in Organic Crystal Structures: Comparison with Distances Expected from Van der Waals Radii. *J. Phys. Chem.* **1996**, *100*, 7384−7391.

(58) Bondi, A. Van Der Waals Volumes and Radii. *J. Phys. Chem.* **1964**, *68*, 441−451.

(59) Cavallo, G.; Metrangolo, P.; Milani, R.; Pilati, T.; Priimagi, A.; Resnati, G.; Terraneo, G. The Halogen Bond. *Chem. Rev.* **2016**, *116*, 2478−2601.

(60) Mitzi, D. B. Synthesis, Crystal Structure, and Optical and Thermal Properties of $(C_4H_9NH_3)_2MI_4$ (M = Ge, Sn, Pb). *Chem. Mater.* **1996**, *8*, 791−800.

(61) Billing, D. G.; Lemmerer, A. Synthesis, Characterization and Phase Transitions of the Inorganic−Organic Layered Perovskite-Type Hybrids $[(C_nH_{2n+1}NH_3)_2PbI_4]$ (n = 12, 14, 16 and 18). *New J. Chem.* **2008**, *32*, 1736−1746.

(62) Safdari, M.; Fischer, A.; Xu, B.; Kloo, L.; Gardner, J. M. Structure and Function Relationships in Alkylammonium Lead(II) Iodide Solar Cells. *J. Mater. Chem. A* **2015**, *3*, 9201−9207.

(63) Im, J.-H.; Chung, J.; Kim, S.-J.; Park, N.-G. Synthesis, Structure, and Photovoltaic Property of a Nanocrystalline 2h Perovskite-Type Novel Sensitizer $(CH_3CH_2NH_3)PbI_3$. *Nanoscale Res. Lett.* **2012**, *7*, 353.

(64) Mao, L.; Stoumpos, C. C.; Kanatzidis, M. G. Two-Dimensional Hybrid Halide Perovskites: Principles and Promises. *J. Am. Chem. Soc.* **2019**, *141*, 1171−1190.

(65) Momma, K.; Izumi, F. Vesta: A Three-Dimensional Visualization System for Electronic and Structural Analysis. *J. Appl. Crystallogr.* **2008**, *41*, 653−658.

(66) Robinson, K.; Gibbs, G. V.; Ribbe, P. H. Quadratic Elongation: A Quantitative Measure of Distortion in Coordination Polyhedra. *Science* **1971**, *172*, 567−570.

(67) In all cases, the photoluminescence (PL) lifetime was <1.5 ns and the PL quantum yield was <1%, which is consistent with other *n* = 1 2D HOIPs (see ref 23).

DOI: 10.1021/acs.chemmater.9b01564
Chem. Mater. XXXX, XXX, XXX−XXX